Virtual-Inerter-Based Dynamic Vibration Absorbers by Using Inertial Actuator with Relative or Absolute Acceleration Feedback

Qibo Mao, Lihua Peng, Jinwu Wu and Xiaotian Li

College of Power and Energy, Nanchang Hangkong University, 696 South Fenghe Avenue, Nanchang, CN-330063, P. R. China. E-mail: qbmao@nchu.edu.cn

(Received 11 October 2025; accepted 28 January 2026)

In this study, the ungrounded and grounded virtual-inerter-based dynamic vibration absorbers (VIDVAs) are proposed by using an inertial actuator with relative or absolute acceleration feedback. The relative acceleration feedback signal is created by using two accelerometers (on the proof-mass and the base of the inertial actuator), whereas the absolute acceleration feedback is generated by an accelerometer on the proof-mass alone. The natural frequencies of the proposed VIDVAs can be tuned by using a virtual inerter without changing its physical design. The tunable VIDVAs in this study aim to reduce resonant vibrations as well as vibrations at a single forcing frequency. The tuning capabilities and control performances of the proposed VIDVAs are investigated numerically and experimentally. The results show that both VIDVAs can reduce resonant vibration significantly, while the grounded VIDVA exhibits broader mode splitting. The experimental results also show that a high level of vibration reduction was achieved by using grounded VIDVA in a wide range of forcing frequencies. Compared to ungrounded VIDVA, the study indicates that the grounded VIDVA is easier to implement and can achieve better control performance.

1. INTRODUCTION

It is well-known that an inerter can exhibit a mass amplification effect.[1–3] The application of inerters to traditional dynamic vibration absorbers (DVAs) has attracted widespread attention, highlighting their potential to significantly improve performance in structural vibration control. Based on different arrangements between inerter, spring and damper, different types of inerter-based DVAs (IDVAs) have been developed in the past 20 years. Generally speaking, the inerter can either be connected to the DVA mass or grounded. In the former configuration (referred to as the ungrounded IDVA in this study), the force exerted by the inerter is proportional to the relative acceleration between the DVA mass and the inerter's terminal attached to the vibrating structure. In the latter configuration (termed as the grounded IDVA), by contrast, the inerter force is proportional to the absolute acceleration of the DVA mass. Typical ungrounded IDVAs and grounded IDVAs are presented in Fig. 1 and 2, respectively. In Figs. 1 and 2, C_n and S_n denote the different types of ungrounded and grounded IDVAs, respectively. Terminal 1 indicates the attachment point to the main structure, while Terminal 2 indicates the attachment point to the IDVA mass (for ungrounded IDVAs) or ground (for grounded IDVAs).

Among the ungrounded IDVAs, the configuration C1 presented in Fig. 1(b) has been the most extensively investigated. For examples, Liu et al.[4] used IDVA-C1 to enhance the dynamical stability of a fluid-conveying pipe. The numerical results showed that the critical pipe flow speed can be significantly increased by using the optimized IDVA-C1. Weber[5] analyzed the control performance of the IDVA-C1 for tall building damping. Wu and Titurus[6] discussed the optimal problem for an IDVA-C1 device linking the two flexible subsystems.

As to grounded IDVAs, the configurations S1 and S6 have received the most attention. The grounded IDVA-S1 shown in Fig. 2(b) (or tuned mass damper inerter, TMDI) is initially proposed by Marian and Giaralis.[7] Numerical results in the literature[7,8] have validated that the IDVA-S1 has superior vibration reduction performances and robustness than classical DVAs. Unlike the ungrounded IDVAs in Fig. 1, where the inerters are connected between the IDVA mass and the main structure, the grounded IDVAs in Fig. 2 have their inerters connected to the ground. Various optimization methods, including the fixed-point theory (FPT),[9] extended FPT,[10] and reliability-based design optimization (RBDO) method,[11] have been applied to the optimal design of IDVA-S1. The numerical results showed that the optimized IDVA-S1 has good control performance under different types of excitations. An extensive review of the current research on IDVA-S1 can be found in the literature.[12,13]

Lazar et al.[14] developed another type of grounded IDVA (see IDVA-S6 in Fig. 2(g)), which is termed as tuned inerter damper (TID). IDVA-S6 (or TID), which can be seen as a variant of IDVA-S1 without the tuned mass, has a similar configuration with the IDVA-S1. The analytical results showed that the IDVA-S6 with a significantly small mass or size can obtain similar control performance to traditional DVAs.[14] Islam and Jangid[15] evaluated the control performance of IDVA-S6 based on numerical search method and also investigated the effect of its physical parameters. Tong et al.[16] presented the optimal natural frequency and damping ratio of the IDVA-S6 in closed-form solution based on the classical and extended FPT.

To achieve better performance, the improved IDVAs with amplified inertances were proposed by using a rhombus truss[17] and a lever.[18] Javidialesaadi and Wierschem[19] proposed inerter-enhanced nonlinear energy sink by replacing the linear spring in the IDVA-S1 with a nonlinear one. Recently, two-DOF IDVAs were also developed to further enhance the control performances.[20,21]

Notice that the control performance of the passive IDVAs is restricted to a fixed frequency band. If the passive ID-

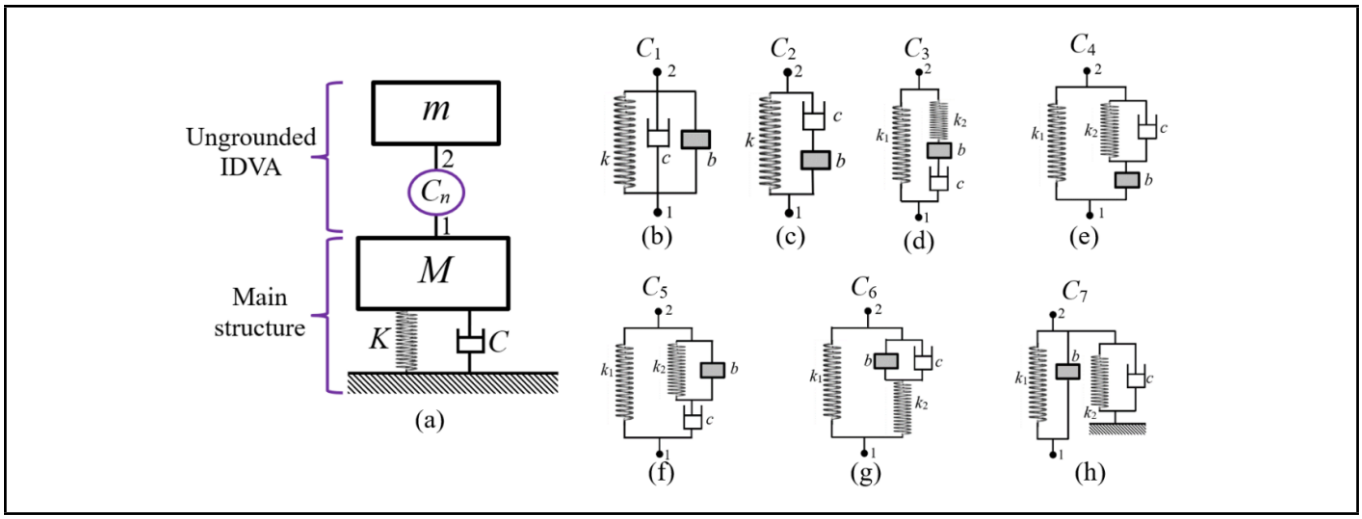

Figure 1. Schematic plot of examples for ungrounded IDVAs.

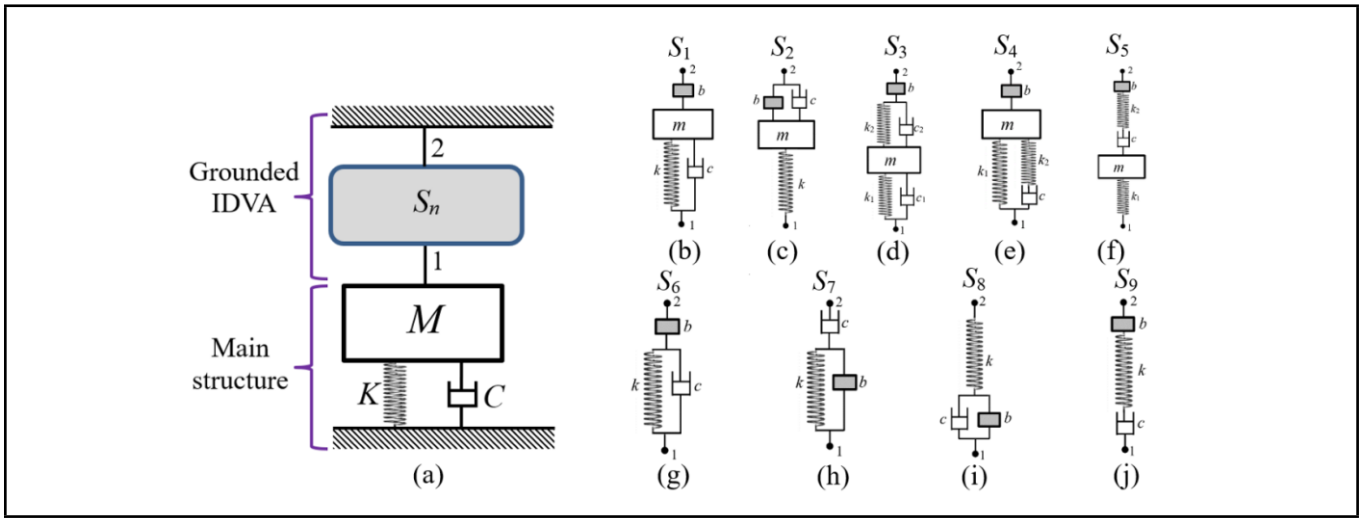

Figure 2. Schematic plot of examples for grounded IDVAs.

VAs are not optimally tuned, or if the structural excitation frequency changes, their control performance will degrade. To overcome this problem, different types of semi-active inerters (tunable inerters) or active inerters were also proposed to make the inertance adjustable. The methods to make the inertance changeable include the continuously variable transmission (CVT),[22] controllable-inertia flywheels[23] and tunable ball-screw inerter.[24] Zhao et al.[25] experimentally investigated active inerters based on collocated reactive actuator and force sensor. Arandia-Kresic et al.[26] proposed an active IDVA-S1 based on voice coil actuator and relative acceleration feedback. Dogan et al.[27] developed different types of active ungrounded IDVAs by using proof-mass actuator with relative displacement feedback. A recent overview of semi-active inerters is presented in the paper by Tran et al.[28]

The aforementioned research collectively indicates that IDVAs can achieve a significant enhancement in performance over classic DVAs. However, the most relevant research is basically theoretical or numerical. Experimental research on IDVAs is still lacking, particularly for grounded configurations, in which the inerters should be grounded to achieve optimal control performance.[29,30]

To address this gap, a tunable VIDVA by using inertial actuator is proposed in this study. The inertial actuator is typically employed as a control source in active vibration control (AVC) systems. The stability and control performance can be improved in AVC if the inertial actuator has a lower natural frequency. Unlike previous studies which have focused on reducing the natural frequency of the inertial actuator by using inerter in AVC system,[31–34] the inertial actuator in this study is used to realize tunable ungrounded and grounded IDVAs with virtual inerter based on active control method. Two control methods are considered. For the first control method, two accelerometers are mounted on both proof-mass and base of the inertial actuator. This arrangement creates the relative acceleration feedback loop that generates the ungrounded virtual inerter effect. For the second method, the accelerometer on the inertial actuator's proof-mass is used to generate a negative absolute acceleration feedback control loop that produces grounded virtual inerter. The tunable VIDVAs in this study aims reduce resonant vibrations as well as vibrations at a single forcing frequency. The tuning capabilities and control performances of the proposed VIDVAs are evaluated numerically and experimentally.

The remainder of this study is organized as follows: the dynamic modeling of the proposed VIDVAs is presented in Section 2. Section 3 analyzes and compares the control performances of the proposed grounded and ungrounded VIDVAs.

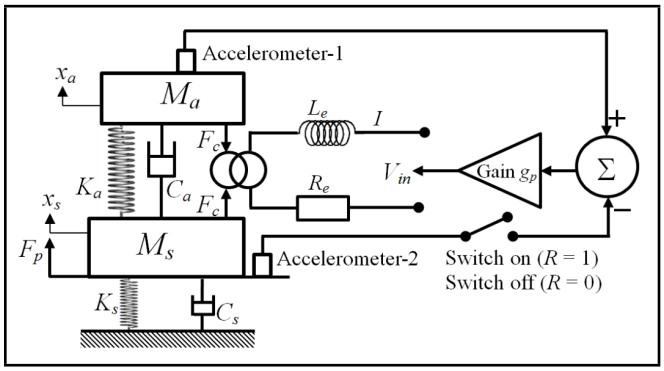

Figure 3. A damped SDOF system controlled by an inertial actuator-based VIDVA

In Section 4, experiments are performed to validate the proposed VIDVAs control performance. Main conclusions and findings are drawn in Section 5.

2. SYSTEM DESCRIPTION AND MATHEMATICAL MODEL

2.1. System Overview

The proposed VIDVA by using inertial actuator with acceleration feedback loop is illustrated in Fig. 3. A linear two-DOF model was used to identify the performances for VIDVAs. The primary system was modelled as a damped single-degree-of-freedom (SDOF) system. M, K and C represented mass, stiffness and damping, respectively. Subscript a and s indicated the inertial actuator and primary system, respectively. The displacements of the inertial actuator mass and the SDOF mass were x_a and x_s, respectively. A disturbance force F_p is applied on the SDOF mass. In the electrical domain, L_e, R_e and I were the inductance, resistance and current of the coil. V_{in} is the control voltage applied to the coil.

A relative or absolute acceleration feedback loop was implemented to impose the virtual inerter. If the switch in Fig. 3 is on $(R = 1)$, the inertial actuator was driven by a control voltage V_{in} proportional to the relative acceleration between the actuator and the primary structure. Conversely, if the switch is off $(R = 0)$, the inertial actuator used the absolute acceleration of its proof-mass as feedback signal. It is well-known that a passive inertial actuator can be viewed as a traditional DVA.[35] By combining this actuator with a variable virtual inerter element, the VIDVA can be established.

2.2. System Model

The equations of motions in the Laplace domain, for proof-mass M_a and SDOF mass M_s, and the electrical circuit behaviour shown in Fig. 3, can be represented as:[31,33,35]

$$M_a s^2 X_a + C_a s(X_a - X_s) + K_a(X_a - X_s) = Bl \cdot I; \quad (1)$$

$$M_s s^2 X_s + C_a s(X_s - X_a) + C_s s X_s + K_a(X_s - X_a) + K_s X_s = F_p - Bl \cdot I; \quad (2)$$

$$L_e s I + R_e I = V_{in} - Bl \cdot s(X_a - X_s); \quad (3)$$

$$F_c = -Bl \cdot I; \quad (4)$$

where s was the Laplace variable. F_c was the control force produced by the current I flowing through the coil. Bl was the electromagnetic coupling coefficient.

The relative or absolute acceleration is used as the feedback control signal. The control voltage V_{in} in the Laplace domain can be written as:

$$V_{in} = s^2(X_a - RX_s) \cdot g_p, \qquad (R = 1 \text{ or } 0); \quad (5)$$

where g_p was the acceleration feedback gain. $R = 1$ indicates that the relative acceleration was used, and $R = 0$ indicates the absolute acceleration.

Substituting Eq. (5) into Eq. (3), the current I flowing through the coil can be written as:

$$I = \frac{s^2(X_a - RX_s)}{sL_e + R_e} g_p - \frac{Bl \cdot s(X_a - X_s)}{sL_e + R_e}. \quad (6)$$

Substituting Eq. (6) into Eq. (5), the control force F_c in Fig. 3 and Eq. (4) can be written as:

$$F_c = -Bl \cdot I = \underbrace{\frac{-Bl}{sL_e + R_e} g_p \cdot s^2(X_a - RX_s)}_{\text{Inter force}} + \underbrace{\frac{Bl}{sL_e + R_e} \cdot s(X_a - X_s)}_{\text{Damping force}}; \quad (7)$$

where $s^2(X_a - RX_s)$ was the relative/absolute acceleration, $s(X_a - X_s)$ was the relative velocity.

According to the definition of the inerter,[1,2] it means that the control force F_c can be seen as the sum of a virtual damping $Bl^2/(sL_e + R_e)$ and a virtual inerter with inertance $-g_p Bl/(sL_e + R_e)$. Clearly, the virtual damping is independent of the control gain g_p. Notice that the term sL_e can be neglected because the coil inductance L_e in inertial actuator is normally sufficiently small.[31,35] It means that the virtual damping and inertance can be approximately equal to Bl^2/R_e and $-g_p Bl/R_e$, respectively. It should be noticed that the virtual inertance in Eq. (7) does not depend on the controlled SDOF system, it depends only on the properties of inertial actuator and feedback gain. It means that the proposed VIDVAs could be used to control the structure with unknown deterministic structural parameters.

From Fig. 3 and Eq. (5), it can be found that the relative acceleration measured by two accelerometers was used as the feedback signal if $R = 1$. It means that the inerter force in Eq. (7) is proportional to the relative acceleration. It will be referred to as ungrounded VIDVA in this study, as shown in Fig. 4(a). Clearly, the proposed ungrounded VIDVA was equal to IDVA-C1 in Fig. 1(b) with additional damping. While one end of the inerter is grounded if $R = 0$, it will be referred to as grounded VIDVA, as shown in Fig. 4(b). It should be noticed that the proposed grounded VIDVA is difference to IDVA-S1 in Fig. 2(b), because there is additional virtual grounded inerter on main structure.

From Eq. (7), it can be found that the feedback gain g_p influences the inertance of the virtual inerter. It can also be found that the inertance was positive if the negative feedback gain was used. Consequently, the dynamic behaviour of the VIDVA can be modified by using different feedback gain g_p.

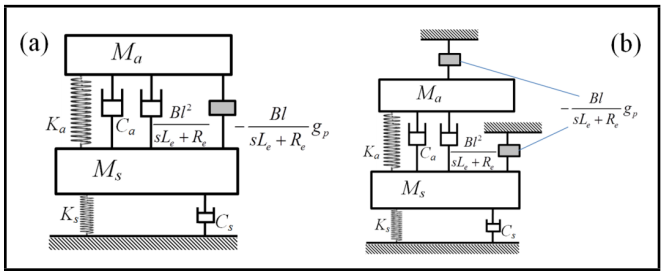

Figure 4. (a) Ungrounded VIDVA based on the relative acceleration feedback; (b) Grounded VIDVA based on the absolute acceleration feedback.

Table 1. The physical parameters of the VIDVA.

Notation	Value	Unit
M_a	0.078	kg
K_a	3.525×10^4	N/m
C_a	5.1	Ns/m
R_e	7.4	Ω
L_e	0.05×10^{-3}	H
Bl	4.6	N/A
M_s	0.78	kg
K_s	1.7625×10^5	N/m
C_s	7.4	Ns/m

Substituting Eq. (6) into Eq. (1) and (2), yields:

$$M_a s^2 X_a + \left(C_a + \frac{Bl^2}{L_e s + R_e}\right) s(X_a - X_s) + K_a(X_a - X_s) - \frac{s^2(X_a - RX_s)Bl}{L_e s + R_e} g_p = 0; \quad (8)$$

$$M_a s^2 X_a + \left(C_a + \frac{Bl^2}{L_e s + R_e}\right) s(X_s - X_a) + C_s s X_s + K_a(X_s - X_a) + K_s X_s + \frac{s^2(X_a - RX_s)Bl}{L_e s + R_e} g_p = F_p. \quad (9)$$

From Eq. (8), the vibration transmissibility function T of the VIDVA can be obtained:

$$T = \frac{X_a}{X_s} = \frac{\left(C_a + \frac{Bl^2}{L_e s + R_e}\right) s + K_a - s^2 g_p R \frac{Bl^2}{L_e s + R_e}}{M_a s^2 + \left(C_a + \frac{Bl^2}{L_e s + R_e}\right) s + K_a - s^2 g_p \frac{Bl^2}{L_e s + R_e}} = \frac{B - s^2 g_p RC}{A - s^2 g_p C}; \quad (10)$$

where $A = M_a s^2 + \left(C_a + \frac{Bl^2}{L_e s + R_e}\right) s + K_a$, $B = \left(C_a + \frac{Bl^2}{L_e s + R_e}\right) s + K_a$, $C = \frac{Bl^2}{L_e s + R_e}$.

Clearly, for a given inertial actuator, the vibration transmissibility T in Eq. (10) was determined solely by the feedback gain g_p. The vibration transmissibility will be used to evaluate the dynamic response of the VIDVAs under different feedback gain.

The closed-loop acceleration frequency response function (FRF) of the main structure, which was used to evaluate the VIDVA's control performance, can be derived from Eqs. (8) and (9), yields:

$$H_{CL} = \frac{s^2 X_s}{F_p} = \frac{(A - s^2 g_p C)s}{AD - B^2 + s^2 g_p (BC + (BC - AC)R - CD)}; \quad (11)$$

where $D = M_a s^2 + \left(C_a + C_s + \frac{Bl^2}{L_e s + R_e}\right) s + (K_a + K_s)$.

The control system's stability can be analyzed by applying the Nyquist criterion to its open-loop FRF. The open-loop FRF in Nyquist format, from VIDVA voltage input to signal output from the accelerometers, can also be obtained from Eq. (8)

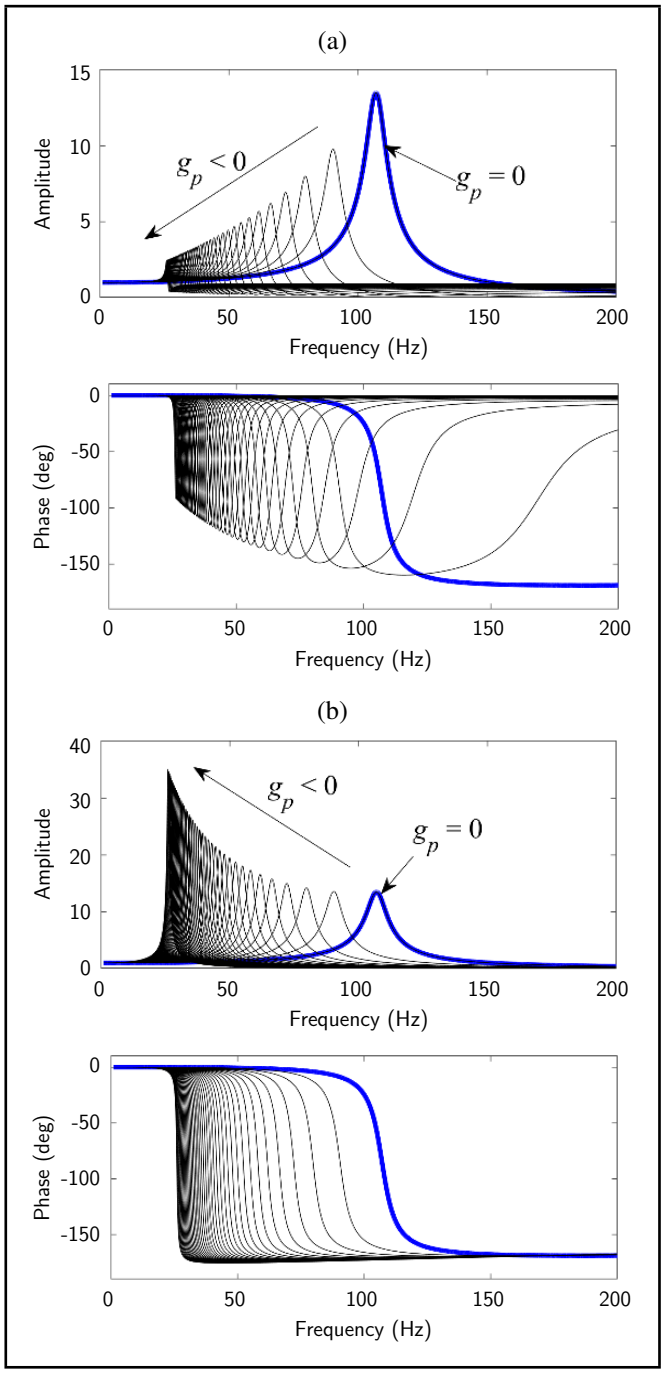

Figure 5. The vibration transmissibility with different gains gp for (a) ungrounded VIDVA and (b) grounded VIDVA.

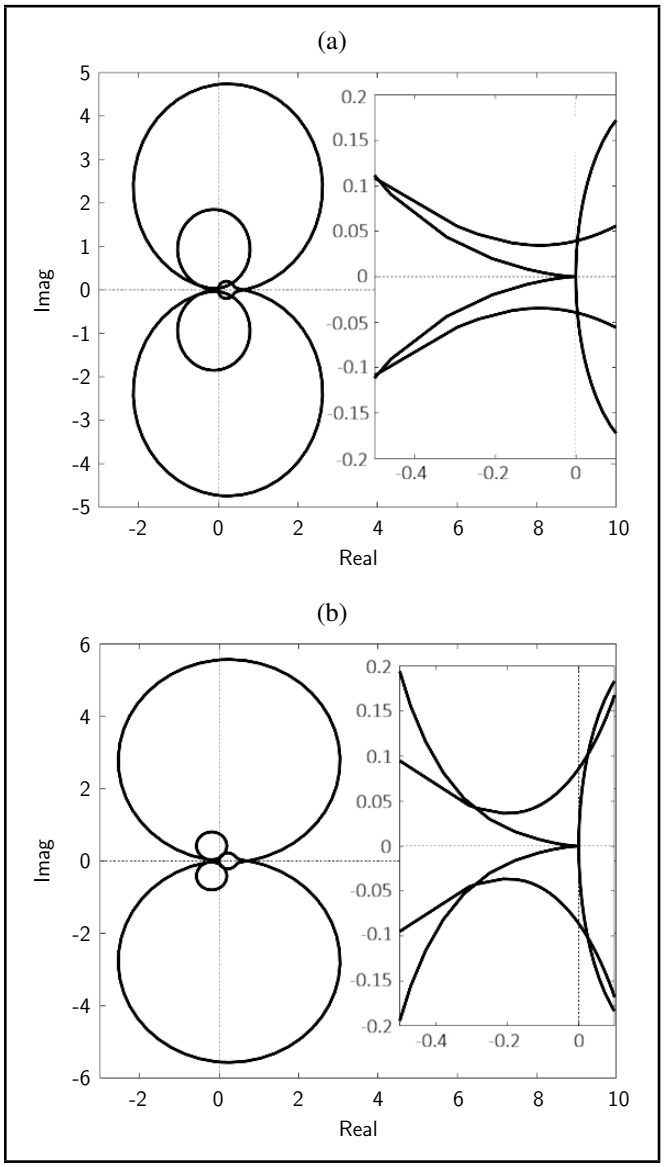

Figure 6. The Nyquist plots with zoomed area around the origin for the open-loop FRFs for (a) ungrounded VIDVA and (b) grounded VIDVA.

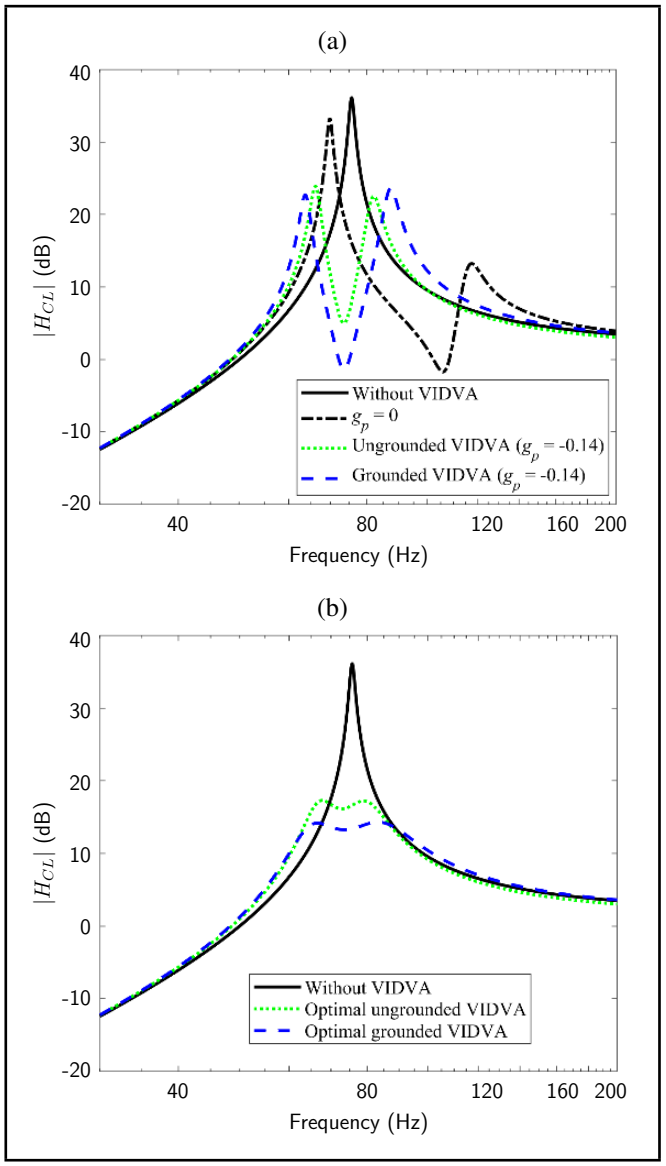

Figure 7. The control performances for VIDVAs (a) when natural frequencies of the VIDVAs are tuned to the natural frequency of the SDOF system; (b) with optimal natural frequencies and damping ratios based on H_2 optimization.

and (9), yields:

$$H_{OL} = \frac{s^2(X_a - RX_s)}{V_{in}} = \frac{CD - BC - (BC - AC)R}{AD - B^2} s^2. \quad (12)$$

3. THE DYNAMIC RESPONSES AND CONTROL PERFORMANCES OF THE VIDVAS

This section numerically presents the tuning capability and control performance of the proposed VIDVAs. Table 1 lists the physical parameters of the proposed VIDVAs and SDOF system for the simulation study.

As discussed in Section 2, the acceleration feedback gains can be used to modify the dynamic responses of the VIDVAs. Prior to their deployment as vibration control devices, it is essential to evaluate the tuning capability of the proposed VIDVAs.

Figure 5 depicts the vibration transmissibility function T of the VIDVAs under different feedback gains. As presented in Fig. 5, when the acceleration feedback gain $g_p = 0$, the VIDVA acted as a passive DVA with the natural frequency of 106.7 Hz. It was clear that the amplitude of transmissibility T at the natural frequency for the ungrounded VIDVA is a decreasing function with respect to negative feedback control gain, as illustrated in Fig. 5(a). Due to the parallel-connected virtual inerter (see Fig. 4(a)), the anti-resonant frequency can be found in transmissibility curves for ungrounded IVDA. In contrast, the amplitudes of the transmissibility T for the grounded VIDVA were increasing due to the ground virtual inerter effect of the absolute acceleration feedback. Furthermore, if the negative acceleration feedback gain g_p was raised, the natural frequencies for both ungrounded and grounded VIDVAs will be shifted to low frequency.

The control stabilities for both VIDVAs were studied by applying the Nyquist criterion to the open-loop FRFs in Eq. (12). Figure 6 shows Nyquist plots of the FRF between the voltage applied to the inertial actuator and the relative acceleration (for ungrounded VIDVA) or absolute acceleration of the proof-mass (for grounded VIDVA). From Fig. 6, it is visible that the instability Nyquist point (-1, 0) will not be not en-

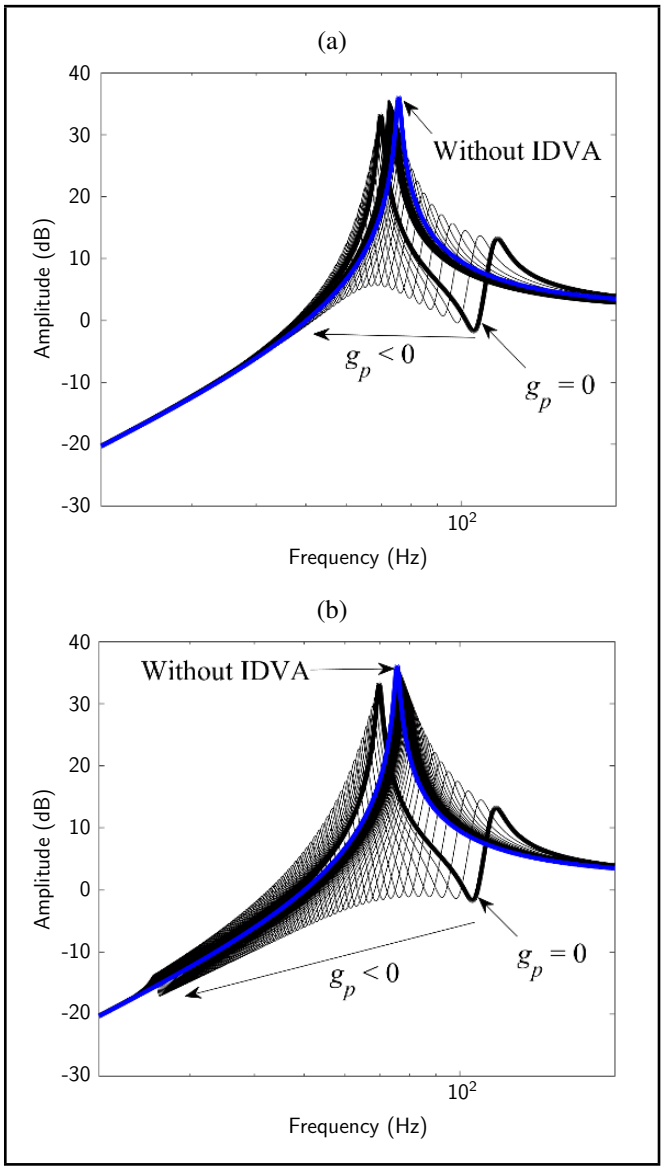

Figure 8. the SDOF responses with (a) ungrounded VIDVA and (b) grounded VIDVA under different feedback gains.

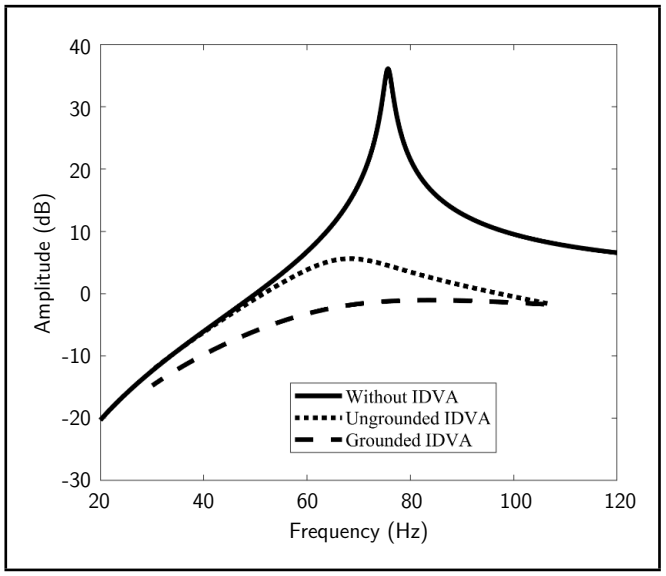

Figure 9. The control performances for VIDVAs when the natural frequencies of the VIDVAs are tuned to the forcing frequency.

circled, because the Nyquist plots for both cases do not pass through negative real axis. It means that the ideal ungrounded and grounded VIDVAs are unconditionally stable under negative acceleration feedback gains.

Notice that the VIDVAs proposed in this study had the tunable inertances, the natural frequencies of the VIDVAs can be tuned to the targeted structural resonance for the resonant response reduction. The VIDVA can also be tuned to the excitation frequency for the controlling of the forcing frequency response.

First, the control performance of the VIDVAs for structural resonant response mitigation based on Eq. (11) was analyzed. Figure 7 shows the control performances for the proposed VIDVAs. In Fig. 7(a), the natural frequencies of the VIDVAs were tuned to natural frequency of the SDOF system. One can observe that the control performances for both VIDVAs improved significantly when the VIDVA's natural frequency was tuned from 106.7 Hz to 76.7 Hz (the resonance frequency of the SDOF system). Two new resonance peaks appear because the damping ratios for both VIDVAs were not optimized. These new peaks were approximately 12.1 dB lower than the resonant peak of the SDOF system. Comparing ungrounded and grounded VIDVAs results shown in Fig. 7(a), it is clear that the grounded VIDVA has a wider peak distance. To further compare the control performances for ungrounded and grounded VIDVAs, Fig. 7(b) shows the control performances for both VIDVAs with optimal natural frequencies and optimal damping ratios by using H_2 optimization method. It can be found that grounded VIDVA has better control performance compared to ungrounded VIDVA (3.1 dB improvement).

Next, the control performances of the VIDVAs for the structural response at different forcing frequencies are discussed. Figure 8 shows the SDOF responses with ungrounded and grounded VIDVAs under different feedback gains. Blue thick lines in Fig. 8(a) and (b) indicate the response of the SDOF system without VIDVA. Black thin lines corresponded to closed-loop FRFs of SDOF system with VIDVAs for equally spaced values of feedback gain from 0 to –2. Analyzing the shapes of these FRFs indicates that the response of the SDOF system is significantly influenced by the feedback gain. To further present benefits of the proposed VIVDAs with tunable inertance based on different feedback gain. Assuming the SDOF system was excited by a sinusoidal signal with unit input force, then the natural frequencies of the VIDVAs were tuned to the forcing frequency by carefully setting the feedback gain. The control performances for both VIDVAs at forcing frequency can be obtained by connecting the response points at each excitation frequency, as presented in Fig. 9. Clearly, the grounded VIDVA demonstrates superior control performance compared to its ungrounded counterpart. It can also be found that both VIDVAs can reduce the amplitude of the SDOF response significantly in the considered range of the forcing frequencies. The grounded VIDVA can significantly reduce the SDOF response for all forcing frequencies. However, the ungrounded VIDVA cannot improve the vibration reduction below 50 Hz. The results in Fig. 9 confirm that the proposed grounded VIDVA exhibits a superior control performance than ungrounded VIDVA due to the virtual grounded inertance effects.

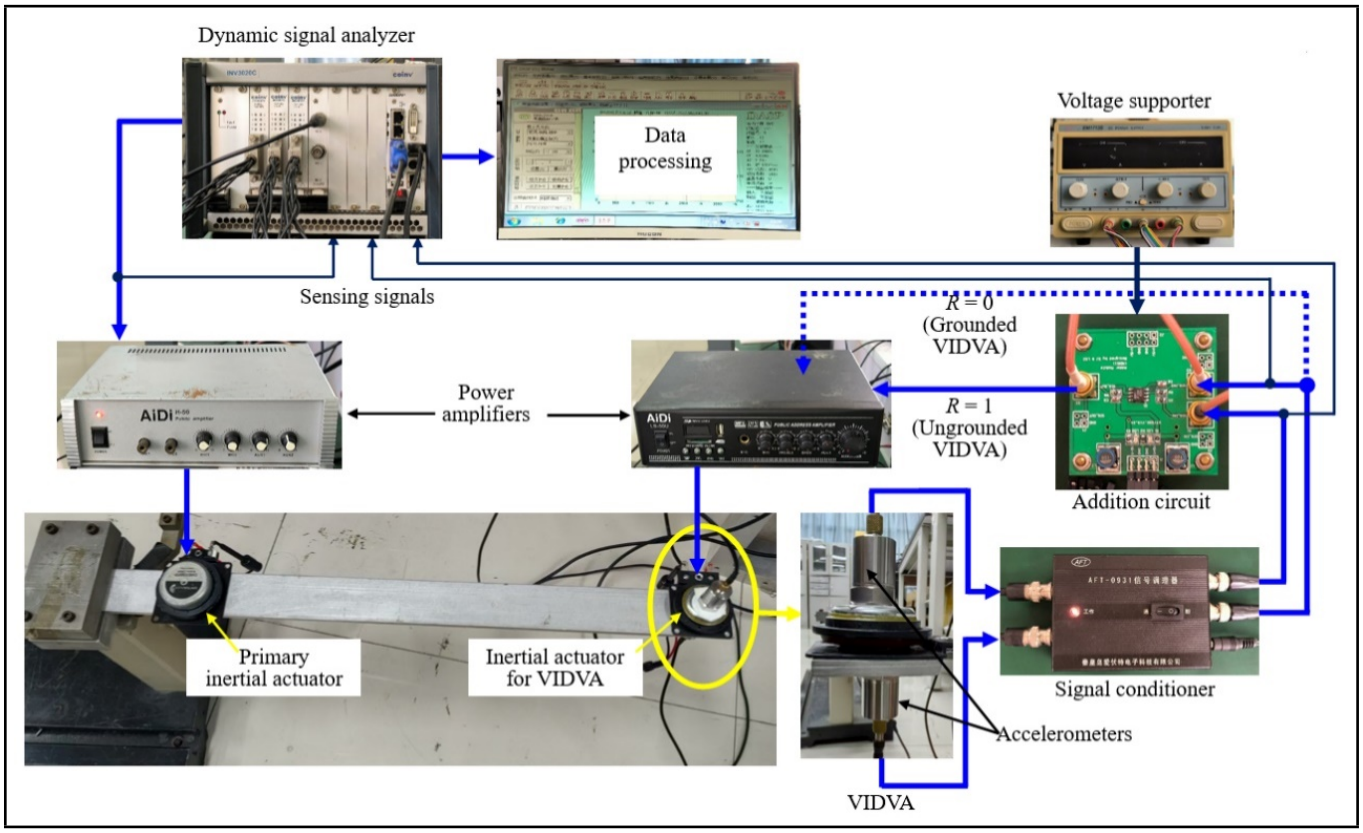

Figure 10. The experimental setup.

4. EXPERIMENTAL SETUP AND RESULTS

4.1. Experimental Setup

This section aims to experimentally validate the proposed VIDVAs, the experimental tests were performed, which is presented in Fig. 10. A cantilever aluminium beam was used as the primary structure. The dimensions of the beam were 500 × 50 × 6 mm. The beam was excited by using an inertial actuator (Dayton Audio DAEX58FP exciter) near the clamped end. This study considered only the beam's second bending mode. Thus, the beam with single-mode can be modeled as a SDOF system.

Another inertial actuator (VISATON EX45S exciter) installed at the free end of the beam was used to design the VIDVAs. Two YD-186 accelerometers (from Sinocera Piezotronics Inc.) were glued on the proof-mass and at the center of control inertial actuator location (on the bottom of the beam). These accelerometers were used to obtain proof-mass and base accelerations, respectively. For grounded VIDVA, the proof-mass accelerometer was used to provide the feedback signal. For ungrounded VIDVA, notice that there is 180° phase difference between the output signals of two accelerometers. An addition circuit was used to acquire the relative acceleration as the feedback signal. The control scheme is also presented in Fig. 10. Clearly, both ungrounded and grounded VIDVAs can be implemented with the same hardware by simply switching between relative and absolute acceleration feedback. To the best of our knowledge, the experimental control performance comparison between ungrounded and grounded IDVAs has not been reported.

The physical parameters of the EX45S inertial actuator (including the accelerometer weight on proof-mass) are listed in Table 1; these parameters were the same as those used in the numerical calculations. The absolute or relative acceleration signal through a low-cost power amplifier was used to drive the control inertial actuator. By shifting the power amplifier gains (feedback gains), the dynamic response of the proposed VIDVAs can be experimentally evaluated. By using a COINV dynamic signal analyzer, the vibration transmissibility functions for the ungrounded and grounded VIDVAs were experimentally measured. The dynamic signal analyzer was also used to acquire the closed-loop FRFs between input voltage and output of the accelerometer on the beam. The measured closed-loop FRFs were applied to check the control performance of the VIDVAs.

4.2. Experimental Results

For ideal condition, the proposed VIDVAs are unconditional stable (see Fig. 6). However, due to the time delay introduced by feedback loop, the power amplifier dynamic and measurement noise, etc., the maximum feedback gains for practical VIDVAs are limited. The measured open-loop frequency responses in Nyquist format for VIDVAs are presented in Fig. 11. From Fig. 11, it can be found that Nyquist plots for both IVDVAs cross the negative real axis. However, the crossing point on the negative real axis is more closer to the origin for the grounded IVDVA than for the ungrounded one. This implies that the grounded VIDVA possesses superior stability margins, allowing for the application of a much higher feedback gain to achieve a lower natural frequency.

The measured vibration transmissibility functions of the ungrounded and grounded VIDVAs with different negative feedback gains are shown in Fig. 12. Comparing the experimental result in Fig. 12 to numerical one in Fig. 5, a good agreement in terms of general trend can be found. According to the plots

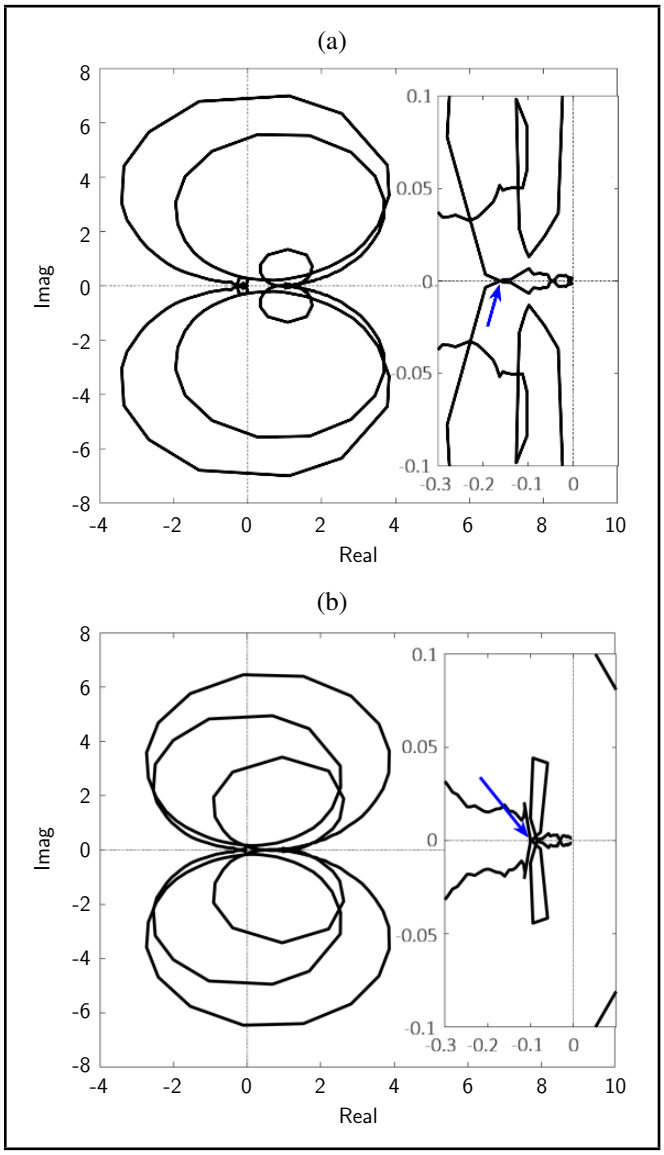

Figure 11. The measured Nyquist plots with zoomed area around the origin for the open-loop FRFs for (a) ungrounded VIDVA and (b) grounded VIDVA. (The blue arrows indicate the crossing point on the negative real axis.)

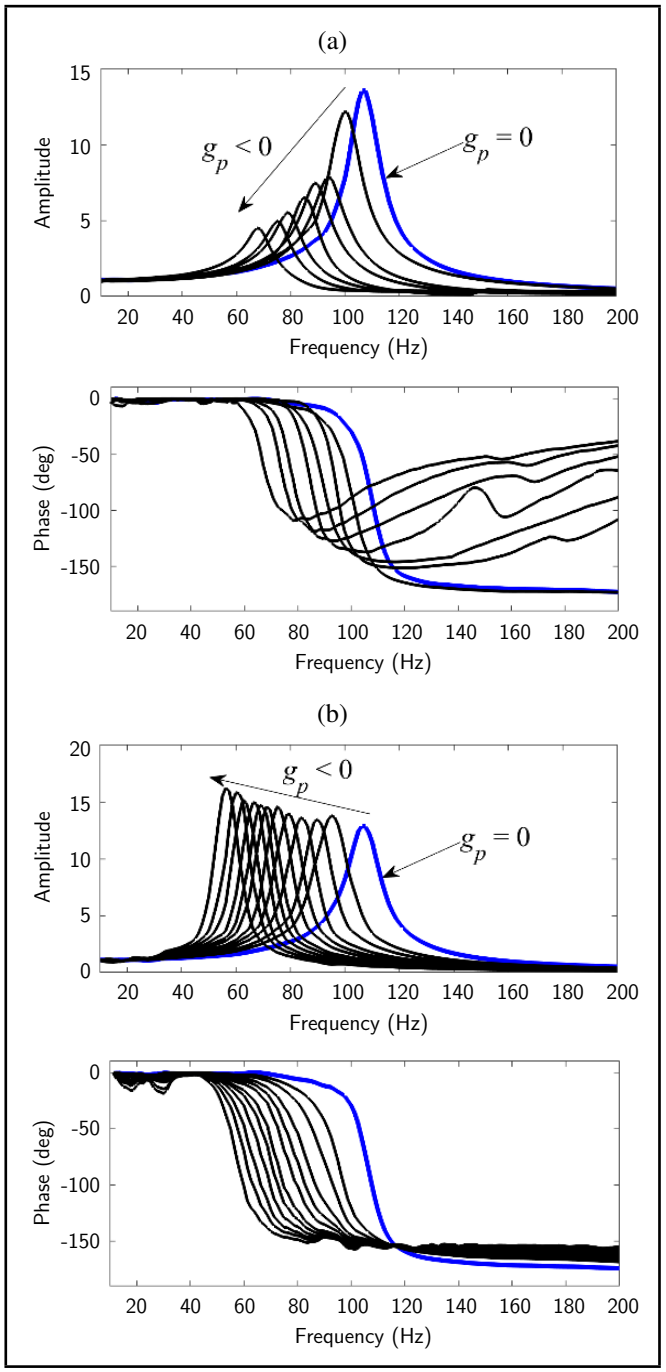

Figure 12. The measured FRFs of the velocity transmissibility of the IA under different power amplifier gains: (a) ungrounded VIDVA and (b) grounded VIDVA.

in Fig. 12, the experimentally achieved lowest natural frequencies are 67.5 Hz for the ungrounded VIDVA and 56 Hz for the grounded VIDVA under maximum feedback gain. This represents a considerable frequency downshift of 39.2 Hz and 50.7 Hz from the original natural frequency of 106.7 Hz, respectively. The experimental results presented in Fig. 12 confirm that the proposed VIDVAs can modify the dynamic responses significantly by using relative or absolute acceleration feedback loop.

By using the experimental rig presented in Fig. 10, the control performance of the VIDVAs in terms of the measured closed-loop FRFs at the VIDVA location are evaluated.

First, the VIDVAs were employed to suppress vibrations for the second mode of the beam. The VIDVAs were tuned to 88.8 Hz to coincide with the second natural frequency of the beam. Figure 13 presents the acceleration responses of the beam without VIDVAs, with passive absorber ($g_p = 0$) and with the ungrounded and grounded VIDVAs. Clearly, when the inertial actuator is used as a passive DVA ($g_p = 0$), only 5.1 dB reduction can be achieved around the second mode because the inertial actuator is not matched to the targeted mode. However, when the ungrounded and grounded VIDVAs is tuned to 88.8 Hz, the closed-loop responses are reduced about 15.4 dB around the second beam mode. It should be noted that the damping ratio of the inertial actuator used in this study is 4.86%, the two new damped resonance peaks were observed at 72.5 Hz and 142.5 Hz for the ungrounded VIDVA, and at 61.3 Hz and 156.3 Hz for the grounded VIDVA. It is clear that the grounded VIDVA exhibits a wider peak separation and a deeper dip around 88.8 Hz than the ungrounded one. It means that the grounded VIDVA can obtain better control performance if the damping ratio is optimized. This will be considered in the future work.

Unlike conventional mechanical inerters, which typically have only a single, fixed configuration, the inertances of the

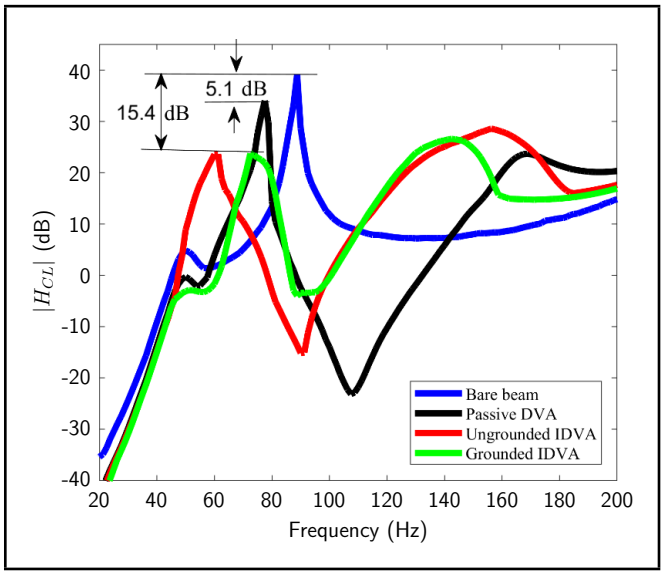

Figure 13. Measured closed-loop FRFs without IDVA, with passive absorber and with the ungrounded and grounded VIDVAs.

virtual inerters of the proposed VIDVAs are programmable; their adjustment can be easily achieved by tuning the power amplifier gains. To further investigate the control performance of the VIDVAs, Fig. 14 presents the time response of the beam with passive DVA, ungrounded and grounded VIDVAs under different forcing frequencies. The connection of responses at each excitation frequency are presented in Fig. 15. For comparison, the responses of the bare beam at frequencies from 65 Hz to 105 Hz (equally spaced) are also presented. From Fig. 14 and 15, both VIDVAs can effectively control the responses of the beam from 70 Hz to 87.5 Hz when the VIDVAs are tuned to the forcing frequency based on the tunable inerter. Furthermore, the grounded VIDVA has superior vibration reduction performances than ungrounded VIDVA or passive DVA. However, the ungrounded VIDVA could perform worse than the passive DVA at 100 Hz (around natural frequency of inertial actuator). This phenomenon is consistent with the numerical calculation results in the work of Weber et al.[29]

5. CONCLUSIONS

In this study, the ungrounded and grounded VIDVA by using inertial actuator with relative and absolute acceleration feedback are presented. The main advantage of the proposed VIDVAs is that the natural frequency of the VIDVAs can be easily changed by imposed a tunable virtual inerter. With an example of a cantilever beam, the control performances of the VIDVAs are experimentally compared and verified. Two experiments including control of the responses of the cantilever beam at resonance frequency and forcing frequency are depicted. The experimental results show that: (1) both VIDVAs can reduce vibration by approximately 15.4 dB around the beam's second mode, while the grounded VIDVA exhibits broader mode splitting; (2) The substitution of an ungrounded VIDVA with a grounded configuration results in a performance enhancement of 8 dB to 12 dB for vibration control at a single forcing frequency.

Unlike mechanical grounded inerter which may be very difficult to realize, the implementation of the proposed grounded VIDVA is simpler, as it requires only a single accelerometer installed on the inertial actuator. Notice that virtual inerter value is only a function of the properties of inertial actuator and feedback gain (see Eq. (7)), the proposed grounded VIDVA could be easily expanded to suppress vibrations in more complicated structures.

ACKNOWLEDGEMENTS

This work was sponsored by the National Natural Science Foundation of China (no. 12364058) and the Jiangxi Provincial Natural Science Foundation Project of China (no. 20252BAC250009).

REFERENCES

[1] Smith M. C. The inerter: A retrospective, *Annual Review of Control, Robotics, and Autonomous Systems*, **3** (1), 361–391, (2020). https://doi.org/10.1146/annurev-control-053018-023917

[2] Wagg D. J. A review of the mechanical inerter: historical context, physical realisations and nonlinear applications, *Nonlinear Dynamics*, **104**, 13–34, (2021). https://doi.org/10.1007/s11071-021-06303-8.

[3] Ma R., Bi K. and Hao H. Inerter-based structural vibration control: a state-of-the-art review, *Engineering Structures*, **243**, 112655, (2021). https://doi.org/10.1016/j.engstruct.2021.112655

[4] Liu Z., Tan X., Liu X., Chen P., Yi K., Yang T., Ni Q. and Wang L. Dynamical stability of cantilevered pipe conveying fluid with inerter-based dynamic vibration absorber, *CMES—Computer Modeling in Engineering & Sciences*, **125** (2), 495–514, (2020). https://doi.org/10.32604/cmes.2020.012030

[5] Weber F. TMD-inerter for tall building damping: approximate closed-form solution, performance and conclusions, *Buildings*, **15**, 1829, (2025). https://doi.org/10.3390/buildings15111829

[6] Wu J. and Titurus B. Frequency analysis of two subsystems coupled by a spring-inerter-damper device and its application to continuous system for vibration control, *Journal of the Franklin Institute*, **362**, 107567, (2025). https://doi.org/10.1016/j.jfranklin.2025.107567

[7] Marian L. and Giaralis A. Optimal design of a novel tuned mass-damper-inerter (TMDI) passive vibration control configuration for stochastically support-excited structural systems, *Probabilistic Engineering Mechanics*, **38**, 156–164, (2014). https://doi.org/10.1016/j.probengmech.2014.03.007

[8] Pietrosanti D., Angelis M. D. and Basili M. Optimal design and performance evaluation of systems with Tuned Mass Damper Inerter (TMDI), *Earthquake Engineering & Structural Dynamics*, **46**, 1367–1388, (2017). https://doi.org/10.1002/eqe.2861

[9] Tong S., Zeng J., Wang Y., Yu S. and Wen H. Optimal design of tuned mass damper inerter (TMDI) parameters for enhanced vibration reduction in damped

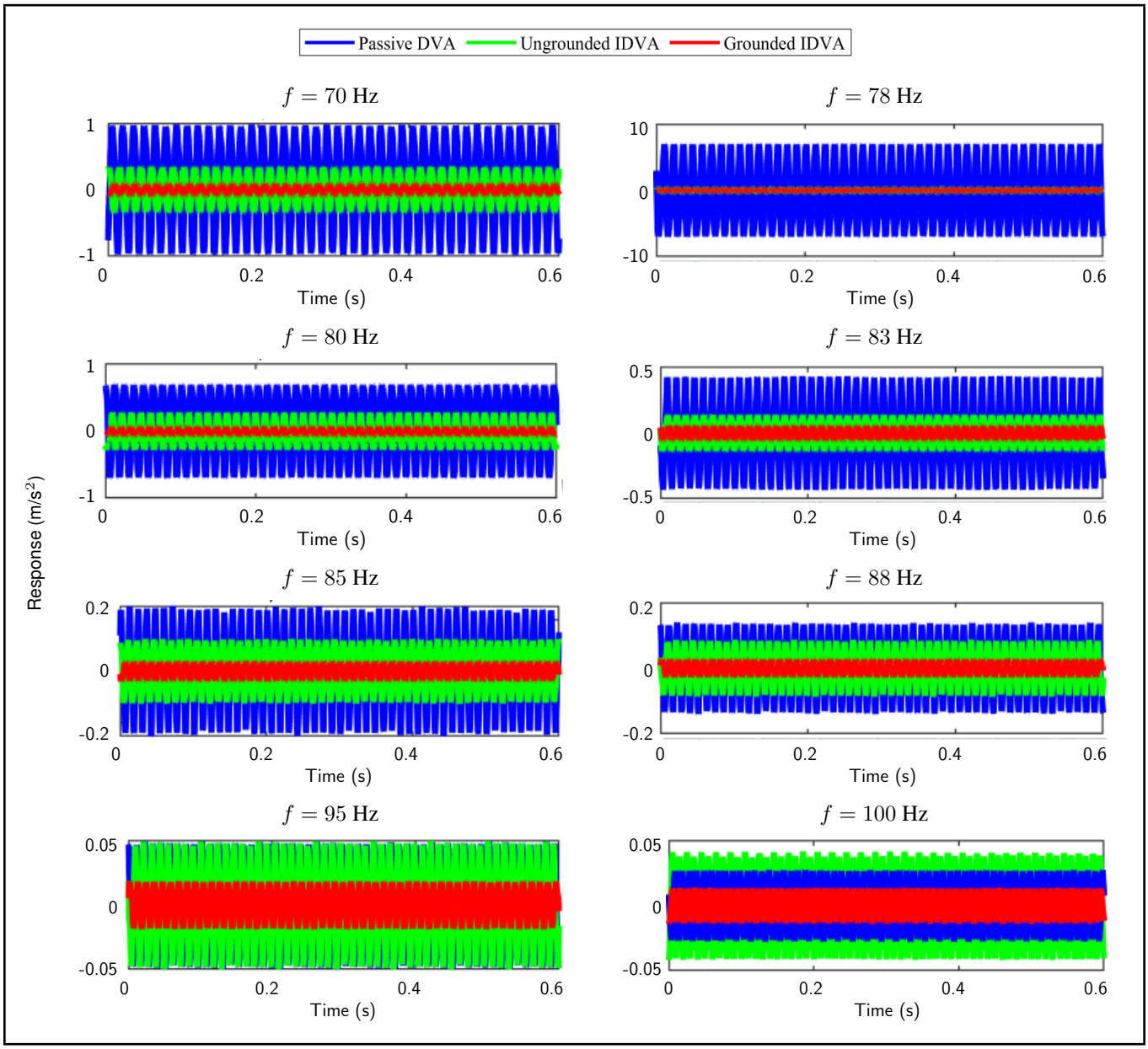

Figure 14. The time response of the beam with passive DVA ($g_p = 0$), ungrounded and grounded VIDVA under different forcing frequencies.

structures: An analytical and numerical study, *Journal of Building Engineering*, **107**, 112768, (2025). https://doi.org/10.1016/j.jobe.2025.112768

[10] Kendo-Nouja B., Baduidana M., Kenfack-Jiotsa A. and Nzengwa R. Vibration reduction of primary structure using optimum grounded inerter-based dynamic vibration absorber, *Archive of Applied Mechanics*, **94** (1), 137–156, (2024). https://doi.org/10.1007/s00419-023-02513-1

[11] Peng Y. and Sun P. Reliability-based design optimization of tuned mass-damper-inerter for mitigating structural vibration, *Journal of Sound and Vibration*, **572**, 118166, (2024). https://doi.org/10.1016/j.jsv.2023.118166

[12] Kang X., Huang Q., Wu Z., Tang J., Jiang X. and Lei S. A review of the tuned mass damper inerter (TMDI) in energy harvesting and vibration control: designs, analysis and applications, *CMES—Computer Modeling in Engineering & Sciences*, **139** (3), 2361–2398, (2024). https://doi.org/10.32604/cmes.2023.043936

[13] Konar T. and Ghosh A. D. Tuned mass damper inerter for seismic control of multi-story buildings: ten years since inception, *Structures*, **63**, 106459, (2024). https://doi.org/10.1016/j.istruc.2024.106459

[14] Lazar I. F., Neild S. A. and Wagg D. J. Using an inerter-based device for structural vibration suppression, *Earthquake Engineering & Structural Dynamics*, **43**, 1129–1147, (2014). https://doi.org/10.1002/eqe.2390

[15] Islam N. U. and Jangid R. S. Optimum parameters of tuned inerter damper for damped structures, *Journal of Sound and Vibration*, **537**, 117218, (2022). https://doi.org/10.1016/j.jsv.2022.117218.

[16] Tong S., Zeng J., Miao Z. and Chen G. Parameter optimization of tuned inerter damper for vibration suppression in structures with damping, *Journal of Sound and Vibration*, **597**, 118827, (2025). https://doi.org/10.1016/j.jsv.2024.118827

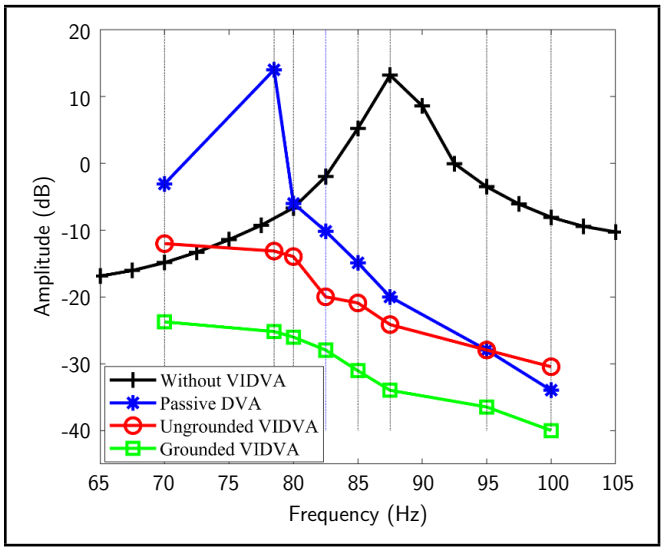

Figure 15. The connection of beam responses at each excitation frequency.

[17] Alotta G. and Failla G. Improved inerter-based vibration absorbers, *International Journal of Mechanical Sciences*, **192**, 106087, (2021). https://doi.org/10.1016/j.ijmecsci.2020.106087

[18] Su N., Bian J., Chen Z. and Xia Y. A novel lever-type inerter-based vibration absorber, *International Journal of Mechanical Sciences*, **254**, 108440, (2023). https://doi.org/10.1016/j.ijmecsci.2023.108440

[19] Javidialesaadi A. and Wierschem N. E. An inerter-enhanced nonlinear energy sink, *Mechanical Systems and Signal Processing*, **129**, 449–454, (2019). https://doi.org/10.1016/j.ymssp.2019.04.047

[20] Barredo E., Zhao Z., Mazon-Valadez C., Larios J. G. M. and Maldonado I. A. A grounded inerter-based oscillating TMD for suppressing harmonic and random vibrations, *International Journal of Mechanical Sciences*, **254**, 108438, (2023). https://doi.org/10.1016/j.ijmecsci.2023.108438

[21] Akbari M., Falborski T. and Jankowski R. Optimal design TID controller with filter for multi-storey buildings equipped with active tendons and double-tuned mass damper inerter under near-field earthquakes, *Journal of Building Engineering*, **111**, 113244, (2025). https://doi.org/10.1016/j.jobe.2025.113244

[22] Brzeski P., Lazarek M. and Perlikowski P. Experimental study of the novel tuned mass damper with inerter which enables changes of inertance, *Journal of Sound and Vibration*, **404**, 47–57, (2017). https://doi.org/10.1016/j.jsv.2017.05.034

[23] Hu Y., Chen M. Z. Q., Xu S. and Liu Y. Semi-active inerter and its application in adaptive tuned vibration absorbers, *IEEE Transactions on Control Systems Technology*, **25** (1), 294–300, (2017). https://doi.org/10.1109/TCST.2016.2552460

[24] Chen M., Li S., Sun Y., Zhao Y. and Wang R. MODWT-based multiscale wavelet LQR strategy and active-inerter tuned mass damper for structural vibration control of floating offshore wind turbines, *Ocean Engineering*, **336**, 121678, (2025). https://doi.org/10.1016/j.oceaneng.2025.121678

[25] Zhao G., Paknejad A., Raze G., Deraemaeker A., Kerschen G. and Collette C. Experimental study on active tuned inerter-dampers: Application to active damping using force feedback, *Journal of Sound and Vibration*, **514**, 116443, (2021). https://doi.org/10.1016/j.jsv.2021.116443

[26] Arandia-Kresic S., Turalija S., Alujevic N. and Vladimir N. Active vibration isolation by emulating the inerter through relative acceleration feedback, *Acta Acustica*, **8**, 49, (2024). https://doi.org/10.1051/aacus/2024047

[27] Dogan H., Ozsoy M., Ozturk E., Wagg D.J. and Sims N. D. Analysis of virtual inerter-based passive absorber for active chatter control, *Journal of Sound and Vibration*, **578**, 118359, (2024). https://doi.org/10.1016/j.jsv.2024.118359

[28] Tran K. T., Jin S., Deng L., Du H., Nguyen H. Q and Li W. Semi-active inerters: a review of the literature, *Frontiers in Materials*, **11**, 1347060, (2024). https://doi.org/10.3389/fmats.2024.1347060

[29] Weber F., Huber P., Borchsenius F. and Braun C. Performance of TMDI for tall building damping, *Actuators*, **9**, 139, (2020). https://doi.org/10.3390/act9040139

[30] Dai J., Xu Z. D. and Gai P. P. Tuned mass-damper-inerter control of wind-induced vibration of flexible structures based on inerter location, *Engineering Structures*, **199**, 109585, (2019). https://doi.org/10.1016/j.engstruct.2019.109585

[31] Zilletti M. Feedback control unit with an inerter proof-mass electrodynamic actuator, *Journal of Sound and Vibration*, **369**, 16–28, (2016). https://doi.org/10.1016/j.jsv.2016.01.035

[32] Alujevic N., Cakmak D., Wolf H. and Jokic M. Passive and active vibration isolation systems using inerter, *Journal of Sound and Vibration*, **418**, 163–183, (2018). https://doi.org/10.1016/j.jsv.2017.12.031

[33] Kras A. and Gardonio P. Active vibration control unit with a flywheel inertial actuator, *Journal of Sound and Vibration*, **464**, 114987, (2020). https://doi.org/10.1016/j.jsv.2019.114987

[34] Cakmak D., Tomicevic Z., Wolf H., Bozic Z. and Semenski D. Stability and performance of supercritical inerter-based active vibration isolation systems, *Journal of Sound and Vibration*, **518**, 116234, (2022). https://doi.org/10.1016/j.jsv.2021.116234

[35] Mao Q., Yuan W. and Wu J. Design and experimental study of a multiple-degree-of-freedom vibration absorber by using an inertial actuator, *International Journal of Structural Stability and Dynamics*, **24** (1): 2450006, (2024). https://doi.org/10.1142/S0219455424500068